Theory and simulation of time-fractional fluid diffusion in porous media

2013 J. Phys. A: Math. Theor. 46 345501

(http://iopscience.iop.org/1751-8121/46/34/345501)

J. Phys. A: Math. Theor. **46** (2013) 345501 (23pp) doi:10.1088/1751-8113/46/34/345501

Theory and simulation of time-fractional fluid diffusion in porous media

José M Carcione[1], **Francisco J Sanchez-Sesma**[2], **Francisco Luzón**[3] **and Juan J Perez Gavilán**[2]

[1] Istituto Nazionale di Oceanografia e di Geofisica Sperimentale—OGS, Borgo Grotta Gigante 42c, I-34010 Sgonico, Trieste, Italy
[2] Instituto de Ingenieria, UNAM, Cd. Universitaria, Circuito Escolar s/n, Coyoacán 04510, México D F, Mexico
[3] Departamento de Física Aplicada, Universidad de Almería, Cañada de San Urbano s/n, E-04120 Almería, Spain

E-mail: jcarcione@inogs.it

Received 22 February 2013, in final form 5 July 2013
Published 2 August 2013
Online at stacks.iop.org/JPhysA/46/345501

Abstract
We simulate a fluid flow in inhomogeneous anisotropic porous media using a time-fractional diffusion equation and the staggered Fourier pseudospectral method to compute the spatial derivatives. A fractional derivative of the order of $0 < \nu < 2$ replaces the first-order time derivative in the classical diffusion equation. It implies a time-dependent permeability tensor having a power-law time dependence, which describes memory effects and accounts for anomalous diffusion. We provide a complete analysis of the physics based on plane waves. The concepts of phase, group and energy velocities are analyzed to describe the location of the diffusion front, and the attenuation and quality factors are obtained to quantify the amplitude decay. We also obtain the frequency-domain Green function. The time derivative is computed with the Grünwald–Letnikov summation, which is a finite-difference generalization of the standard finite-difference operator to derivatives of fractional order. The results match the analytical solution obtained from the Green function. An example of the pressure field generated by a fluid injection in a heterogeneous sandstone illustrates the performance of the algorithm for different values of ν. The calculation requires storing the whole pressure field in the computer memory since anomalous diffusion 'recalls the past'.

PACS numbers: 47.10.−g, 47.10.A−, 47.10.ab, 47.11.Bc, 47.11.Kb

1. Introduction

The basic notion of the fractional derivative is widely recognized in science in general and, in particular, in the fields of mathematical physics, engineering and biology. Numerous applications of mathematical memory formalisms to the description of physical phenomena

have been published. We attempt here to recall some contributions, being sure that some work will be unintentionally omitted. Fractional diffusion equations were first derived in the context of a continuous time random walk model by Hilfer and Anton [37] and Compte [21], which since then been widely studied [45]. Importantly, the fractional diffusion equation has been generalized to include space-dependent forcing [2], reactions [27, 36], time-dependent forcing [56], advection and dispersion [4, 54] and space- and time-dependent forcing [35].

Diffusion equations are obtained in poroelasticity and electromagnetism at low frequencies and under certain conditions, by which the inertial terms and displacement currents, respectively, are neglected [12]. In hydrocarbon exploration and production, diffusion equations are mainly used to map the sub-seafloor resistivity [1] and model fluid flow in reservoir rocks [3]. Shapiro *et al* [55] describe the phenomenon of microseismicity caused by fluid injection in boreholes by using the diffusion equation obtained in the low-frequency limit of Biot theory. Indeed, Chandler and Johnson [20] have shown the equivalence between the quasi-static fluid flow and Biot's diffusive wave [12]. Luzón *et al* [44] presented a hybrid method to calculate the total pore pressure variations in poroelastic media around water reservoirs, and applied it to compute these variations around the Itoiz dam (northern Spain).

The classical Darcy's law plays an essential role in describing the flow in a porous medium [3]. It assumes that the permeability is constant during the diffusion process. It may occur that fluids carry solid particles which obstruct the pores or may chemically react with the solid grains. In such cases, the permeability of the matrix changes with time. The time-dependent permeability in the form of a relaxation function accounts for the past values of the pressure field, involving a time convolution. If the relaxation function is expressed as a power law, the convolution can formally be interpreted as a time-fractional derivative. At any instant the diffusion can be affected by the history of pressure and flow [9].

Diffusion-like equations containing fractional derivatives in time and/or in space are usually adopted to the model phenomena of anomalous transport in physics. The time-fractional diffusion-wave equation is obtained by replacing the first-order time derivative in the classical diffusion equation by a derivative of fractional order. The order ν of the time derivative can be any real number between 0 and 2; $\nu = 1$ gives the classical diffusion equation and $\nu = 2$ gives the wave equation. The range [0, 1] corresponds to dispersive anomalous sub-diffusion, while the range [1, 2] corresponds to generalized wave propagation. Several physical phenomena, besides fluid flow, can be described with the fractional diffusion equation, for instance, turbulent plasma, diffusion of carriers in amorphous photoconductors, diffusion in a turbulent flow, vortex dynamics, the chaotic regime of the Josephson junction, a percolation model in porous media, fractal media, various biological phenomena and finance problems. Fractional models are also used to examine the heat transfer in a biological tissue [39]. In seismology, constant-Q wave propagation corresponds to time-fractional equations with ν close to 2 [8]. Its finite-difference (FD) implementation in 2D heterogeneous media has been performed by Carcione *et al* [14] and Carcione [13].

Fractional derivatives can be computed with the Grünwald–Letnikov (GL) and central-difference approximations, which are the extensions of the standard FD approximation for derivatives of integer order [13, 14, 29, 31]. Unlike the standard operator of differentiation, the fractional operator increases in length as time increases, since it must keep the memory effects introduced by the fractional derivative. Caputo and Carcione [6] used fractional derivatives of the distributed order to model the fatigue of materials, while Caputo *et al* [7] applied fractional derivatives to the propagation of waves in the biological and dissipative media.

In this work, we examine the diffusion process for inhomogeneous anisotropic media. It is a generalization of the theory and numerical method presented in Carcione and Gei [16] to fractional orders of differentiation. With the physics of the phenomenon in mind, we obtain the

time-fractional diffusion equation. Then, we use the approximation based on the GL derivative and verify the accuracy of the time discretization by comparing the exact and the FD phase velocities and attenuation factors. The model is discretized on a regular mesh, and the spatial derivatives are calculated with the Fourier method by using the fast Fourier transform (FFT). This approach is called 'pseudospectral' and it is infinitely accurate for band-limited periodic functions with cut-off spatial wavenumbers smaller than the cut-off wavenumbers of the mesh. On the other hand, Lin and Xu [43] solve the sub-diffusion equation with an FD scheme in time and Legendre spectral methods in space. Since past solutions have to be stored, the use of this highly accurate discretization makes the method efficient in terms of storage. A similar performance is obtained by using the Fourier method, which needs at least two points per minimum wavelength.

We test the modeling algorithms with analytical solutions for 1D and a 2D homogeneous media and illustrate the method in inhomogeneous fractal media.

2. The fractional diffusion equation

When inertial terms are neglected in the governing equations of poroelasticity [12], the remaining equations are diffusion-like. In fact, the quasi-static limit of Biot's equations, to describe the diffusion of the second (slow) compressional mode, is obtained by neglecting the acceleration terms in the equations of momentum conservation, and considering the constitutive equations and Darcy's law [5].

2.1. Biot's classical equation

Biot's relevant stress–strain relation and Darcy's law for inhomogeneous media are given by

$$p = M(\zeta - \alpha_{ij}\epsilon_{ij}), \quad \zeta = -\partial_i w_i \tag{1}$$

and

$$-\partial_i p = \frac{\eta}{\kappa_{(i)}}\partial_t w_i, \quad i = 1, \ldots, 3 \tag{2}$$

(equations (8.399) and (8.401) in Carcione [12]), where p is the fluid pressure, ζ is the variation of fluid content, w_i are the components of the fluid displacement vector relative to the solid, ϵ_{ij} are the components of the strain tensor of the skeleton (matrix), κ_i are the components of the permeability tensor (in its principal system), η is the dynamic viscosity, α_{ij} are components of the effective-stress coefficient matrix (equation (7.139) in Carcione [12]; see below), ∂_i is the spatial derivative with respect to the variable x_i and ∂_t is the time derivative ($(x_1, x_2, x_3) = (x, y, z) = \mathbf{r} = r\hat{\mathbf{r}}$). The stiffness M is

$$M = \frac{K_s}{(1 - K/K_s) - \phi(1 - K_s/K_f)}, \tag{3}$$

where ϕ is the porosity, K_s is the bulk modulus of the solid grains, K_f is the fluid bulk modulus and

$$K = \tfrac{1}{9}[c_{11} + c_{22} + c_{33} + 2(c_{12} + c_{13} + c_{23})] \tag{4}$$

is the bulk modulus of the skeleton, with c_{IJ} being the elastic constants of the (drained) skeleton.

Combining equations (1) and (2) yields the diffusion equation

$$\frac{1}{M}\partial_t p + \alpha_{ij}\partial_t \epsilon_{ij} = \partial_i(a_i \partial_i p), \quad a_i = \frac{\kappa_i}{\eta}, \quad \text{and} \quad i, j = 1, \ldots, 3. \tag{5}$$

In the isotropic case, equation (5) becomes

$$\frac{1}{M}\partial_t p + \alpha \partial_t \epsilon_{ii} = \partial_i \left(a \partial_i p\right), \quad a = \kappa/\eta, \tag{6}$$

where $\alpha = 1 - K/K_s$.

2.2. *Uncoupling fluid flow and deformation*

The fluid pressure is coupled with the strain of the matrix in equations (5) and (6). This makes the problem much more difficult to solve, but there are situations where these field variables can be uncoupled. They occur when the displacement field is irrotational or when the fluid is very compressible [22]. We may avoid such approximation by using a less stringent one. The total stress is

$$\sigma_{ij} = c_{ijkl}\epsilon_{kl} - \alpha_{ij} p \tag{7}$$

(equation (7.132) in Carcione [12]), where σ_{ij} are the components of the total stress tensor and c_{ijkl} are the elastic constants in the four indices notation [34]. Let us assume the case of fluid injection in a borehole, transverse isotropy ($a_2 = a_1$), uniaxial strain conditions and vertical deformations only. This is valid for sub-horizontal layers whose vertical dimension is small compared to their lateral extent. In this case, the only non-zero differential strain is $\mathrm{d}\epsilon_{33}$. Assuming no changes in the vertical stress, we obtain from (7):

$$\mathrm{d}\sigma_{33} = 0 \simeq c_{3333}\mathrm{d}\epsilon_{33} - \alpha_{33}\mathrm{d}p = c_{33}\mathrm{d}\epsilon_{33} - \alpha_{33}\mathrm{d}p. \tag{8}$$

Using this formula, equation (5) becomes

$$\partial_t p = N \Delta_I p, \tag{9}$$

where

$$\Delta_I = \partial_1(a_1\partial_1 p) + \partial_2(a_1\partial_2 p) + \partial_3(a_3\partial_3 p) \quad \text{and} \quad \frac{1}{N} = \frac{1}{M} + \frac{\alpha_{33}^2}{c_{33}} \tag{10}$$

and the subindex '*I*' in the Laplacian indicates that it corresponds to inhomogeneous media, i.e., equation (9) is required when computing diffusion fields using direct methods (FDs, finite elements, pseudospectral methods, etc). The permeability tensor is diagonal with two independent components κ_1 and κ_3, such that

$$a_i = \frac{\kappa_i}{\eta}, \quad i = 1, 3, \tag{11}$$

$$\alpha_{33} = 1 - (2c_{13} + c_{33})/(3K_s), \tag{12}$$

and M is given by (3), with

$$K = \tfrac{1}{9}[2c_{11} + c_{33} + 2(c_{12} + 2c_{13})]. \tag{13}$$

Another similar situation, although uncommon in a borehole, is when the strain tensor is isotropic, i.e., $\mathrm{d}\epsilon_{11} = \mathrm{d}\epsilon_{22} = \mathrm{d}\epsilon_{33} = 0$. It is easy to show that if $\mathrm{d}\sigma_{33} = 0$, we obtain $N = 1/[1/M + \alpha_{33}^2/(2c_{13} + c_{33})]$. Knowledge of N in both cases is useful to quantify the correction to be applied to the fluid-flow equation due to the deformation of the skeleton. More general approaches involving the coupling of a fluid flow and deformation take into account the coupled Biot's equations [32].

We consider the uncoupled case in the rest of the paper, where N, corresponding to uniaxial strain conditions, is used as the stiffness. In this case, we do not assume any restriction about the symmetry of the permeability tensor.

2.3. Generalized Darcy's law and the time-fractional equation

In order to obtain the fractional diffusion equation, we use a generalization of Darcy's law. The mathematical formulation is the same as that used for constant-Q wave propagation [8, 13, 14, 48]. The related viscoelastic equations are

$$\sigma = \psi * \partial_t \epsilon = M_0 \omega_0^{-\beta} \partial_t^{\beta} \epsilon,$$
$$\psi = \frac{M_0}{\Gamma(1-\beta)} \left(\frac{t}{t_0}\right)^{-\beta} H(t), \quad t_0 = 1/\omega_0, \tag{14}$$

where σ is the stress, ϵ is the strain, ψ is the relaxation function, M_0 is a bulk modulus, ω_0 is a reference frequency, β is the order of the derivative, H is the Heaviside function, Γ is Euler's Gamma function and '$*$' denotes time convolution. We use the following formal mathematical analogy:

$$\sigma \to -\partial_i p, \quad \epsilon \to \partial_t w_i, \quad M_0 \to 1/a_i, \quad \beta \to \nu - 1, \tag{15}$$

to obtain

$$-\partial_i p = \psi * \partial_t^2 w_i = \frac{1}{a_i} \omega_0^{1-\nu} \partial_t^{\nu} w_i, \quad \text{where} \quad \psi = \frac{1}{a_i \Gamma(2-\nu)} \left(\frac{t}{t_0}\right)^{1-\nu} H(t). \tag{16}$$

This is a generalization of Darcy's law to include memory effects. The fractional derivative is remembering their past values, which implies that the permeability of the matrix changes during the diffusion process, related to the relaxation function ψ. These changes may occur because the fluids may carry solid particles which obstruct the pores or may chemically react with the matrix. At any instant the diffusion can be affected by the history of pressure and flow.

Taking the divergence of equation (16) and using the stress–strain relation $-\partial_i w_i = p/N$, we obtain the generalization of the diffusion equation (9),

$$\partial_t^{\nu} p + s = N \Delta_I p, \quad 0 < \nu \leqslant 2, \quad a_i = \frac{\kappa_i}{\eta} \omega_0^{\nu-1}, \tag{17}$$

where we have introduced a source term s. These types of equations were studied by Nigmatullin [51], Westerlund [60], Mainardi [46, 47] and recently Hanyga [33]. Another modification was introduced by Caputo and Plastino [9] and Iaffaldano *et al* [38] for isotropic media. A generalization of their equation to anisotropic media can be

$$\partial_t p + s = N[\Delta_I p + \Delta_\gamma \partial_t^{\nu} p], \tag{18}$$

where Δ_γ is similar to Δ_I, but replacing a_i with γ_i, $i = 1$ or 3 (see equation (9)).

If the medium is homogeneous, we can express equation (17) as

$$\partial_t^{\nu} p + s = \Delta_H p, \tag{19}$$

where

$$\Delta_H = b_1 \partial_1^2 + b_2 \partial_2^2 + b_3 \partial_3^2, \quad b_i = N a_i = N \frac{\kappa_i}{\eta} \omega_0^{\nu-1}, \quad i = 1, \ldots, 3, \tag{20}$$

where b_i are the principal components of the hydraulic diffusivity tensor.

3. Plane-wave analysis

Let us assume a kernel of the form $\exp[\mathrm{i}(\omega t - \mathbf{k} \cdot \mathbf{x})]$, where ω is the angular frequency, $\mathbf{k}$ is the complex wavenumber vector and $\mathbf{x}$ is the position vector. Assuming homogeneous fields, we have $\mathbf{k} = k(l_1, l_2, l_3)^{\top}$, where $k = \mathrm{Re}(k) - \mathrm{i}\alpha$, α is the attenuation factor and l_i are the direction cosines defining the propagation direction.

3.1. Dispersion relation and complex velocity

Assuming homogeneous media and substituting the kernel into equation (17), in the absence of the source, gives the dispersion equation

$$(\mathrm{i}\omega)^{\nu} = -\left(b_1 l_1^2 + b_2 l_2^2 + b_3 l_3^2\right)k^2. \tag{21}$$

We define the complex velocity as

$$v_c = \frac{\omega}{k} = (\mathrm{i}\omega)^{1-\nu/2}\sqrt{b_1 l_1^2 + b_2 l_2^2 + b_3 l_3^2}. \tag{22}$$

The same kinematic concepts used in wave propagation (acoustics and electromagnetism) are useful in this analysis [12].

3.2. Phase velocity, attenuation factor and skin depth

The phase velocity and attenuation factor can be obtained from the complex velocity as

$$v_p = \left[\mathrm{Re}\left(v_c^{-1}\right)\right]^{-1} \quad \text{and} \quad \alpha = -\omega\,\mathrm{Im}(v_c^{-1}), \tag{23}$$

respectively, where Re and Im take real and imaginary parts. The skin depth is the distance d for which $\exp(-\alpha d) = 1/e$, where e is Napier's number, i.e., the effective distance of penetration of the signal. Then, $d = 1/\alpha$; $d = \sqrt{2b/\omega}$ for $\nu = 1$ and isotropic media, where $b = \kappa N/\eta$. Using equation (22) yields

$$v_p = [\sin(\pi\nu/4)]^{-1}\omega^{1-\nu/2}\sqrt{b_1 l_1^2 + b_2 l_2^2 + b_3 l_3^2} \tag{24}$$

and

$$\alpha = \frac{1}{d} = \left(\frac{\omega}{v_p}\right)\cot(\pi\nu/4). \tag{25}$$

3.3. Envelope and group velocities

Without loss in generality, let us consider the (x, z)-plane, where $l_2 = 0$, $l_1 = \sin\theta$, $l_3 = \cos\theta$ and $l_1^2 + l_3^2 = 1$. It has been shown by Carcione [10, 12] that the location of the wave front in anisotropic attenuating media is given by the energy velocity, since the concept of group velocity breaks down. Carcione has also shown that the energy velocity can be approximated quite well by the envelope velocity, which is given by (equation (1.146) in Carcione [12])

$$v_{\mathrm{env}} = \sqrt{v_p^2 + \left(\frac{\mathrm{d}v_p}{\mathrm{d}\theta}\right)^2}. \tag{26}$$

Using (24), we obtain

$$v_{\mathrm{env}} = v_p\frac{\sqrt{b_1^2 l_1^2 + b_3^2 l_3^2}}{\left(b_1 l_1^2 + b_3 l_3^2\right)^2} = \frac{\omega^{2-\nu}}{v_p\sin^2(\pi\nu/4)}\sqrt{b_1^2 l_1^2 + b_3^2 l_3^2}. \tag{27}$$

In the isotropic case, $b_1 = b_3$ and $v_{\mathrm{env}} = v_p$. We show below that the envelope velocity is exactly the energy velocity for the equations of the form (17).

On the other hand, the components of the group velocity are equal to the derivative of the frequency ω with respect to the real wavenumber components, i.e., $\partial\omega/\partial\mathrm{Re}(k_i)$. The components are $k_i = kl_i$. The group-velocity vector can be obtained from the dispersion relation as (equation (4.39) in Carcione [12])

$$\mathbf{v}_g = -\left[\mathrm{Re}\left(\frac{\partial F/\partial\omega}{\partial F/\partial k_1}\right)\right]^{-1}\hat{\mathbf{e}}_1 - \left[\mathrm{Re}\left(\frac{\partial F/\partial\omega}{\partial F/\partial k_3}\right)\right]^{-1}\hat{\mathbf{e}}_3, \tag{28}$$

where, from equation (21),

$$F(k_1, k_3) = b_1 k_1^2 + b_3 k_3^2 + (\mathrm{i}\omega)^\nu = 0. \tag{29}$$

We obtain

$$\mathbf{v}_g = \frac{2\omega^{2-\nu}}{\nu\,\mathrm{Re}(\mathrm{i}^{2+\nu} v_c)}(a_1 l_1 \hat{\mathbf{e}}_1 + a_3 l_3 \hat{\mathbf{e}}_3) \tag{30}$$

and

$$v_g = \frac{2\omega^{2-\nu}}{\nu\,\mathrm{Re}(\mathrm{i}^{2+\nu} v_c)}\sqrt{b_1^2 l_1^2 + b_3^2 l_3^2}. \tag{31}$$

In the isotropic case, we have $v_g = 2v_p/\nu$. If $\nu = 2$, we obtain the wave equation and the medium is lossless. Note that only in the isotropic lossless case, we have $v_g = v_p = v_{\mathrm{env}}$. In the anisotropic lossless case, it is $v_g = v_{\mathrm{env}} \neq v_p = v_c$. When the medium is lossy, the group velocity differs from the envelope velocity. The group velocity obtained by Shapiro *et al* [55] differs from (31) in that the factor $\mathrm{Re}(\mathrm{i}^{2+\nu} v_c)$ has been replaced by $|\mathrm{i}^{2+\nu} v_c|$. His approach is to compute the components $\partial\omega/\partial k_i$ and then take the absolute value of the result. Both velocities are similar if the imaginary part of v_c is small compared to its real part. Since $\mathrm{Im}(v_c)/\mathrm{Re}(v_c) = \cot(\pi\nu/4)$, this happens for $\nu = 2$ (wave equation). For $\nu = 1$ the relation is 1, so the two velocities differ.

3.4. Energy velocity, wave front and quality factor

The calculation of the energy velocity requires the establishment of an energy balance equation. Again, we use the fact that diffusion fields can be treated with the same mathematical formulation used for the propagation of waves. The energy balance could be explicitly developed and the energy velocity can be obtained as the energy flux divided by the total energy. For brevity, we use an analogy between equation (5) and that describing the propagation of seismic SH waves. The complex velocity of SH waves, given by equation (4.106) in Carcione [12], is mathematically equivalent to equation (22), provided that we make the following substitutions:

$$p_{66} \to (\mathrm{i}\omega)^{2-\nu} b_1, \quad p_{44} \to (\mathrm{i}\omega)^{2-\nu} b_3, \quad \rho \to 1, \tag{32}$$

where p_{66} and p_{44} are complex and frequency-dependent stiffnesses and ρ is the mass density. The energy velocity is given by equation (4.115) in Carcione [12]. Then, using this equation and the equivalence (32), we obtain

$$\mathbf{v}_e = \frac{\omega^{2-\nu}}{v_p \sin^2(\pi\nu/4)}(b_1 l_1 \hat{\mathbf{e}}_1 + b_3 l_3 \hat{\mathbf{e}}_3), \tag{33}$$

where we have used the property $v_p\,\mathrm{Re}(\mathrm{i}^{2-\nu}/v_c) = 1$. As can be seen by comparison to (27), $v_{\mathrm{env}} = v_e$. Equation (33) provides, in addition, the direction of the energy flux (ray angle),

$$\tan\vartheta = \frac{b_1 l_1}{b_3 l_3} = \frac{\kappa_1}{\kappa_3}\tan\theta. \tag{34}$$

If $\nu = 2$ (lossless case), we have that $v_g = v_e$, while in the pure diffusion case ($\nu = 1$), it is $v_g = 2v_e$. The group- and energy-velocity vectors have the same direction but different magnitude. With the exception of the lossless case, for which the velocity is the same for all the frequencies, the velocity goes from zero at $\omega = 0$ to infinity at $\omega = \infty$. Hence, the definition of the wave front or diffusion front is related to a given frequency. We define the wave front as the location of the tip of the energy velocity vector at unit propagation time.

The quality factor has two definitions in the literature, which give approximately the same value when $Q \gg 1$, as is the case for seismic waves. These definitions are: (i) $Q_1 =$ twice

the potential energy V divided by the dissipated energy D and (ii) $Q_2 =$ the total energy $E = T + V$ divided by D, where T is the kinetic energy. The energies are time averaged over a cycle. Denoting $\beta = \pi\nu/4$, we have $T \propto 1$, $V \propto \cos 2\beta$, $E \propto 1 - \cos 2\beta$ and $D \propto \sin 2\beta$ (see equation (22) and equations (4.112), (4.113) and (4.114) in Carcione 2007).

The first definition gives a quality factor

$$Q_1 = \frac{2V}{D} = \frac{\mathrm{Re}\left(v_c^2\right)}{\mathrm{Im}\left(v_c^2\right)} = -\cot 2\beta \tag{35}$$

(Carcione [12], equation (4.92)), where we have used equation (22). The limit cases of the absence of energy dissipation (the elastic energy is fully stored) and of the absence of energy storage (the elastic energy is fully dissipated) are recovered from (35) for $\beta = \pi/2$ (perfectly elastic solid, $\nu = 2$) and $\beta = \pi/4$ (perfectly viscous fluid, $\nu = 1$), respectively.

The second definition gives

$$Q_2 = \frac{E}{D} = \frac{\mathrm{Re}^2(v_c)}{\mathrm{Im}\left(v_c^2\right)} = \frac{1}{2}\tan\beta, \tag{36}$$

for which $Q = 0$, 1/2 and ∞ for $\nu = 0$, 1 and 2, respectively.

Note that $(E, V, D) \propto (0, 1, 0)$, $(1, 0, 1)$ and $(2, -1, 0)$, for $\nu = 0$, 1 and 2, respectively. Each definition has its own drawback. Q_1 is negative for sub-diffusion ($\nu < 1$), while Q_2 does not vanish for $\nu = 1$.

4. Green's function and the time-domain solution

Let us consider equation (19) and perform the following change of coordinates:

$$x \to x'\sqrt{b_1}, \quad y \to y'\sqrt{b_2}, \quad z \to z'\sqrt{b_3} \tag{37}$$

which transforms Δ_H into a pure Laplacian differential operator. Using equation (37), equation (19) becomes

$$\partial_t^\nu p + s = \Delta' p, \tag{38}$$

where

$$\Delta' = \partial_{1'}^2 + \partial_{2'}^2 + \partial_{3'}^2. \tag{39}$$

The nD Green function is given in Hanyga [33] (equation (A3) with $s = \mathrm{i}\omega$ and $A = 1$),

$$G_{nD}(r') = 2\pi\mathrm{i}\left(\frac{r'^{1-n/2}(\mathrm{i}\omega)^{\nu(n/4-1/2)}}{\mathrm{i}(2\pi)^{n/2+1}}\right) K_{n/2-1}[(\mathrm{i}\omega)^{\nu/2}r'], \tag{40}$$

where

$$\begin{array}{lll} r' = x', & \Delta' = \partial_{1'}^2, & 1\mathrm{D}, \\ r' = \sqrt{x'^2 + z'^2}, & \Delta' = \partial_{1'}^2 + \partial_{3'}^2, & 2\mathrm{D}, \\ r' = \sqrt{x'^2 + y'^2 + z'^2}, & \Delta' = \partial_{1'}^2 + \partial_{2'}^2 + \partial_{3'}^2, & 3\mathrm{D}, \end{array} \tag{41}$$

and K_γ denotes the Macdonald function of order γ. Note that Hanyga [14] (equation 2.1) solves $\partial_t^{2\nu} u = A\Delta u + s$, where u is the unknown variable, A is a constant and s is the source. Moreover, $\Phi = 1$ in his equation (A2) since the initial conditions are zero.

The 1D solution is

$$G_{1D}(r') = (\mathrm{i}\omega)^{-\nu/4}\sqrt{\frac{r'}{2\pi}}K_{-1/2}[(\mathrm{i}\omega)^{\nu/2}r']. \tag{42}$$

In the 2D case ((x, z)-plane)), equation (40) has the solution

$$G_{2D}(r') = \frac{1}{2\pi} K_0[(\mathrm{i}\omega)^{\nu/2} r']. \tag{43}$$

The 3D Green function is

$$G_{3D}(r') = \frac{(\mathrm{i}\omega)^{\nu/4}}{2\pi\sqrt{2\pi r'}} K_{1/2}[(\mathrm{i}\omega)^{\nu/2} r']. \tag{44}$$

When solving the problem with a limited-band wavelet source $s(t)$, the frequency-domain solution is multiplied by the Fourier transform $S(\omega)$. To ensure a real time-domain solution, we consider an Hermitian frequency-domain solution. Finally, the time-domain solution is obtained by an numerical inverse transform.

4.1. Closed-form solutions in the time domain for $\nu = 1$ and $\nu = 2$

If $\nu = 1$, we can express equation (19) as

$$\partial_t g - \Delta' g = \delta(r')\delta(t), \tag{45}$$

whose solution is [19]

$$g = \frac{1}{(4\pi t)^{n/2}} \exp[-r'^2/(4t)] H(t) \tag{46}$$

and

$$r' = \sqrt{\frac{x^2}{b_1} + \frac{y^2}{b_2} + \frac{z^2}{b_3}} \tag{47}$$

(omit the y-term if $n = 2$). The diffusion length vector (L_1, L_2, L_3) is defined as $r' = \sqrt{4t}$. It is obtained from

$$\frac{L_1^2}{b_1} + \frac{L_2^2}{b_2} + \frac{L_3^2}{b_3} = 4t. \tag{48}$$

It is a measure of how far the field has propagated at time t.

If $\nu = 2$, we have

$$\partial_t^2 g - \Delta' g = \delta(r')\delta(t). \tag{49}$$

The 2D solution is

$$g = \frac{1}{2\pi} \frac{H(t - r')}{\sqrt{t^2 - r'^2}} \tag{50}$$

(e.g., Carcione [12], equation (3.197)); $r' = r/c$ when the medium is isotropic, where $c = \sqrt{b}$ is a velocity.

Having the Green function, one can compute the solution for a general source time history $s(t)$ as

$$p = g * s. \tag{51}$$

In particular, for $s = H(t)\delta(\mathbf{r})$ (uniform injection rate), we have for the 3D diffusion case (46)

$$p = \frac{1}{(4\pi)^{3/2}} \int_0^t \frac{1}{\tau^{3/2}} \exp(-r'^2/4\tau)\mathrm{d}\tau = \frac{1}{4\pi r} \mathrm{erfc}\left(\frac{r'}{\sqrt{4t}}\right), \tag{52}$$

where 'erfc' is the complementary error function; $\mathrm{erfc}(q) = 1 - \mathrm{erf}(q) = (2/\sqrt{\pi}) \int_q^\infty \exp(-p^2)\mathrm{d}p$, where 'erf' is the error function.

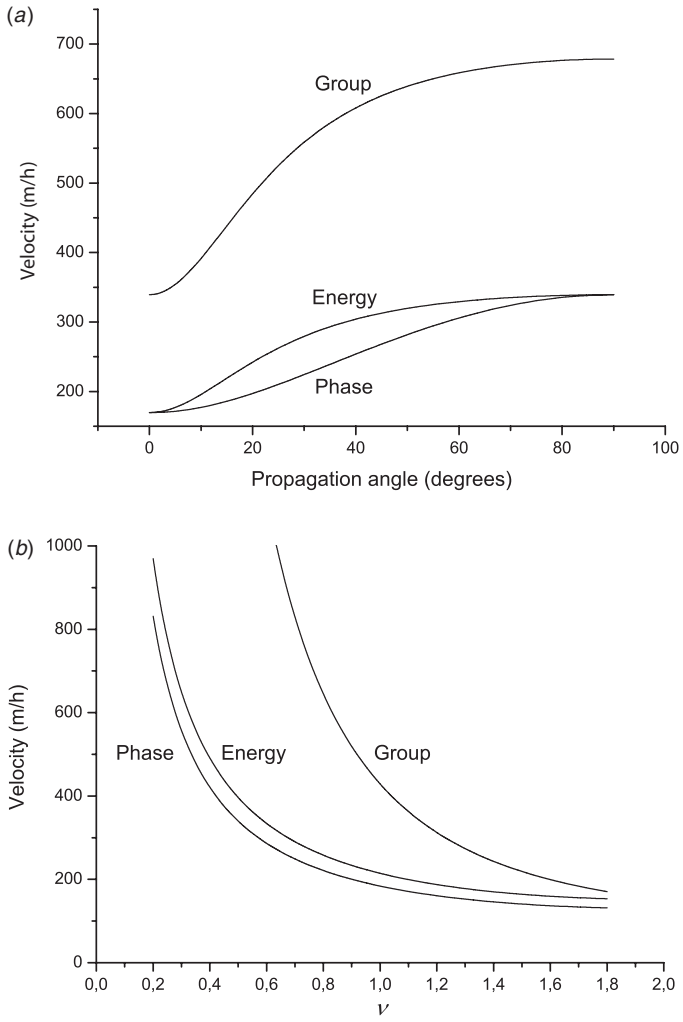

Figure 1. Phase, energy and group velocities as a function of the propagation angle (*a*) and ν (*b*).

5. Numerical algorithm

The most widely used time approximation in fractional calculus is the backward GL derivative. The GL fractional derivative of a function f is

$$h^{\nu}\frac{\partial^{\nu} f(t)}{\partial t^{\nu}} \sim \sum_{j=0}^{J}(-1)^{j}\binom{\nu}{j} f(t-jh), \tag{53}$$

where h is the time step and $J = t/h - 1$. The derivation of this expression can be found, for instance, in Carcione *et al* [14]. The binomial coefficients can be defined in terms of Euler's Gamma function as

$$\binom{\nu}{j} = \frac{\Gamma(\nu+1)}{\Gamma(j+1)\Gamma(\nu-j+1)}$$

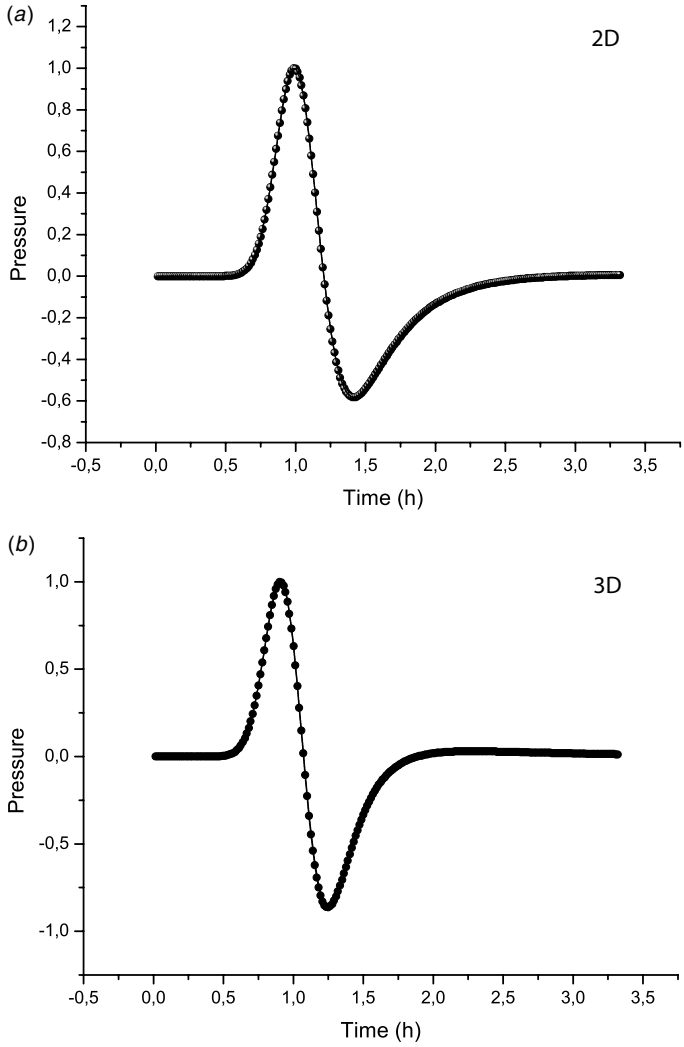

Figure 2. Pressure as a function of time for $\nu = 1$ obtained from the frequency- and-time domain Green's functions (solid and dotted lines, respectively). (*a*) 2D space; (*b*) 3D space.

and can be calculated by a simple recursion formula

$$\binom{\nu}{j} = \frac{\nu - j + 1}{j}\binom{\nu}{j-1}, \qquad \binom{\nu}{0} = 1.$$

If ν is a natural number, we have the classical derivatives. In this case $J = \nu$ in equation (53). The GL approximation is of the order of O(h). The fractional derivative of f at time t depends on all the previous values of f. This is the memory property of the fractional derivative. In our calculations, we consider the whole memory history since for $\nu < 1$ it is not possible to use the short-memory principle, i.e., fewer terms in the sum of equation (53), as can be used in the simulation of wave propagation [14]. Waves 'forget' the past but diffusion fields 'remember' it.

The time discretization of equation (17) for ν close to 1 using the GL derivative is

$$D^{\nu} p^{n-1} + s^{n-1} = N\Delta_I p^{n-1}, \tag{54}$$

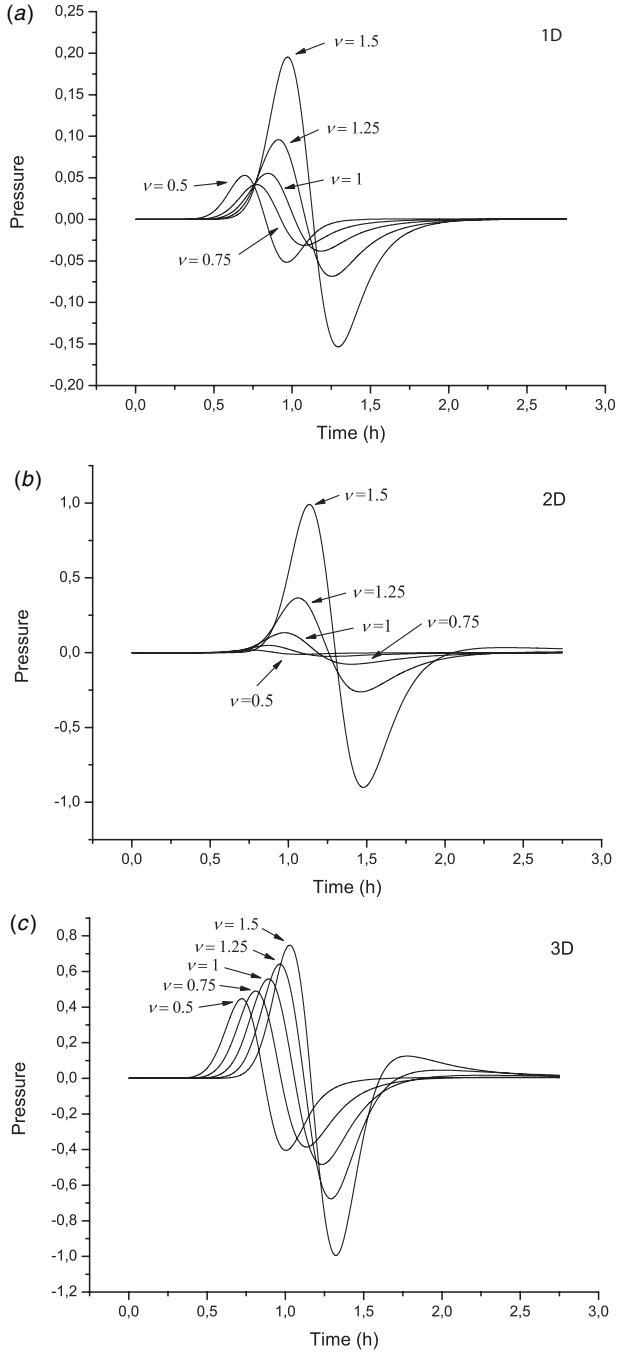

Figure 3. Normalized pressure as a function of time for various values of ν. (*a*) 1D space; (*b*) 2D space; (c) 3D space. In the 1D case, the pressure is divided by ν^4 to enhance the field with lower ν.

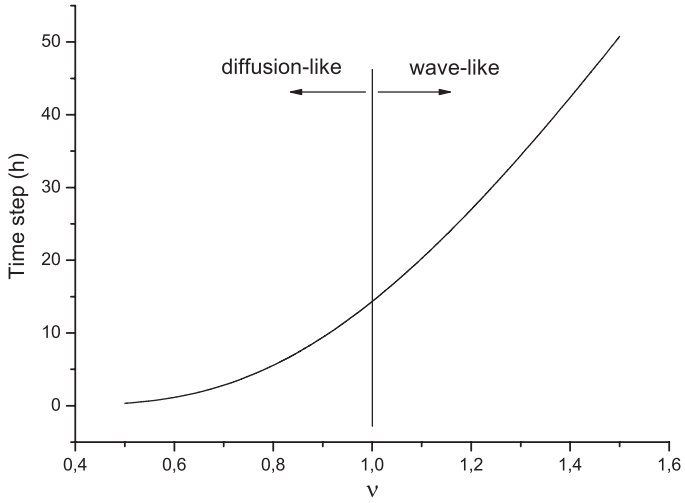

Figure 4. Time step as a function of ν.

where

$$h^{\nu} D^{\nu} p^{n-1} = p^n + \sum_{j=1}^{J} (-1)^j \binom{\nu}{j} (p^{n-j} - p^0). \tag{55}$$

Combining equations (54) and (55), p^n can be computed from its past values p^{n-j} as

$$p^n = h^{\nu}(N\Delta_I p^{n-1} - s^{n-1}) - \sum_{j=1}^{J} (-1)^j \binom{\nu}{j} (p^{n-j} - p^0). \tag{56}$$

The accuracy and stability of this algorithm are analyzed in appendix A. It is important to note that equations (14), (16) and (17) correspond to a time-fractional differential equation in the Caputo sense and the GL derivative corresponds to a time-fractional derivative in the Riemann–Liouville (RL) sense, see for example [30], equation (5.2). Here, we consider the causal events $p(t) = 0$ for $t < 0$. If $p(t = 0^+) = 0$, the RL and Caputo derivatives are the same. If $p(t = 0+)$ is a constant p^0, then the Caputo derivative is equal to the RL derivative of $[p(t) - p^0]$. In equations (55) and (56), the subtraction of p^0 reflects the subtraction of $p(t = 0^+)$ to obtain the Caputo fractional derivative. However, our diffusion equation is such that we initiate the perturbation with a source (a fluid injection in practice) and therefore the initial condition $p(0^+) = 0$ and the two derivatives coincide. In the case of non-zero initial conditions, the numerical implementation of the Caputo fractional derivative can be found in Diethelm *et al* [23] and Diethelm [24].

The spatial derivatives are calculated with the Fourier method by using the FFT [12, 40]. The Fourier pseudospectral method has spectral accuracy for band-limited signals. Then, the results are not affected by spatial numerical dispersion. In the case of inhomogeneous media, the algorithm employs the staggered Fourier method. Staggered operators evaluate derivatives between grid points. For instance, if Δx is the grid (cell) size and k_1 is the wavenumber component, a phase shift $\exp(\pm \mathrm{i} k_1 \Delta x/2)$ is applied when computing the x-derivative. Then, $\partial_1 a_1 \partial_1$ is calculated as $D_1^- a_1 D_1^+$, where $D_1^{\pm}$ is the discrete operator and $\pm$ refers to the sign of the phase shift. The spatial differentiation requires the interpolation of the material properties at half grid points.

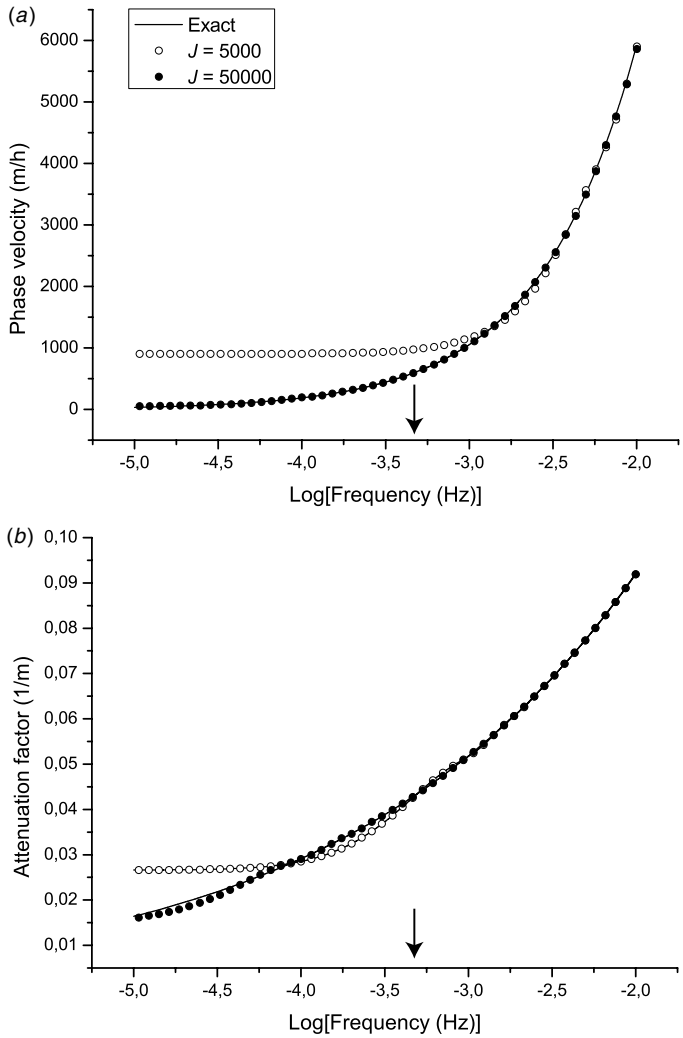

Figure 5. FD phase velocity (*a*) and attenuation factor (*b*) (symbols) as a function of frequency compared to the exact values (solid line) for different memory lengths, J, $\nu = 0.5$ and $h = 0.2$ s. The arrow indicates the peak source frequency used in the simulations.

6. Results

In order to illustrate the physics, we use the following material properties: $c_{11} = 35$ GPa, $c_{12} = 3$ GPa, $c_{13} = 5$ GPa, $c_{33} = 25$ GPa, $K_s = 40$ GPa, $K_f = 2.25$ GPa, $\phi = 0.25$, $\kappa_1 = 0.2$ D, $\kappa_3 = 0.05$ D, $\eta = 1$ cP and $\omega_0 = \pi \times 0.001$ Hz. Figures 1(*a*) and (*b*) show the velocities as a function of the propagation angle and ν, respectively, for $\omega = \omega_0$. In figures 1(*a*), it is $\nu = 1$ and in (*b*) it is $\vartheta = \pi/4$, which gives $\theta = 14^{\rm o}$ (see equation (34)). As can be seen, the group velocity is quite different from the energy velocity. An evaluation of the correct velocity is made qualitatively when computing the transient response as a function of ν (see figure 3 below).

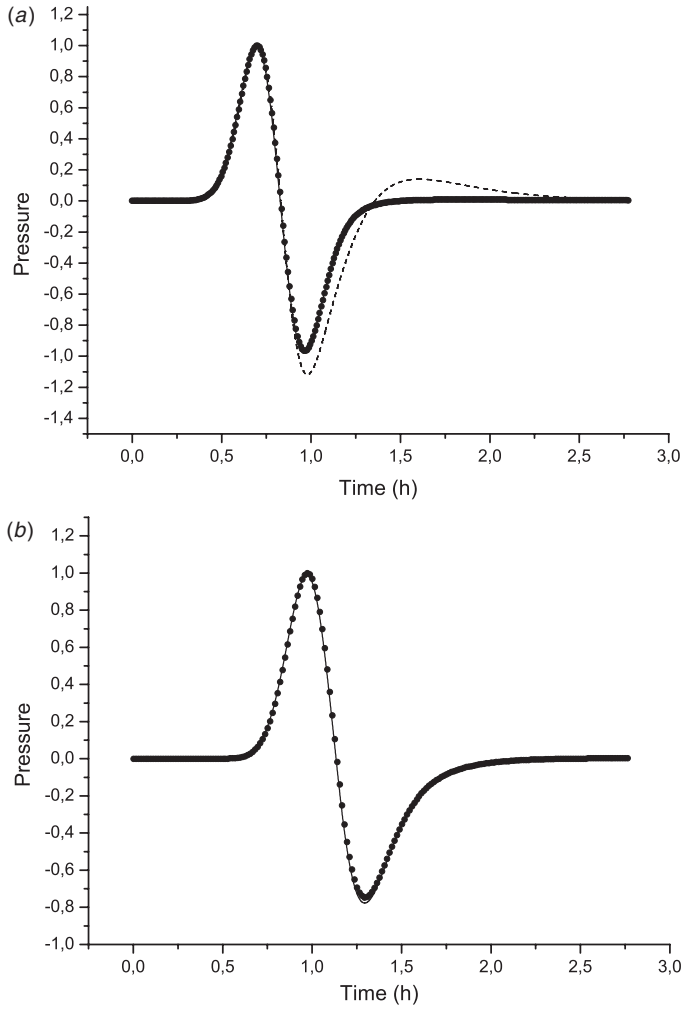

Figure 6. Comparison between the 1D analytical and numerical solutions (solid line and dots) for $\nu = 0.5$ (*a*) and $\nu = 1.5$ (*b*). A memory length $J = 50\,000$ time steps has been used in (*a*). The dashed line corresponds to $J = 5000$.

To compute the transient responses, we use a Ricker wavelet of the form

$$w(t) = \left(a - \frac{1}{2}\right)\exp(-a), \quad a = \left[\frac{\pi\,(t - t_s)}{t_p}\right]^2, \tag{57}$$

where t_p is the period of the wave (the distance between the side peaks is $\sqrt{6}t_p/\pi$) and we take $t_s = 1.4t_p$. Its frequency spectrum is

$$W(\omega) = \left(\frac{t_p}{\sqrt{\pi}}\right)\bar{a}\exp(-\bar{a} - \mathrm{i}\omega t_s), \quad \bar{a} = \left(\frac{\omega}{\omega_p}\right)^2, \quad \omega_p = \frac{2\pi}{t_p}. \tag{58}$$

The peak frequency is $f_p = 1/t_p$.

We test the analytical solutions (40) with equation (46) for $\nu = 1$. The 2D and 3D Green functions are multiplied by the Ricker wavelet (58) and then transformed to the time domain using a discrete Fourier transform. We use the previous material properties. The Green functions are computed using a time step of 100 s at $x = z = 100$ m and a source peak frequency

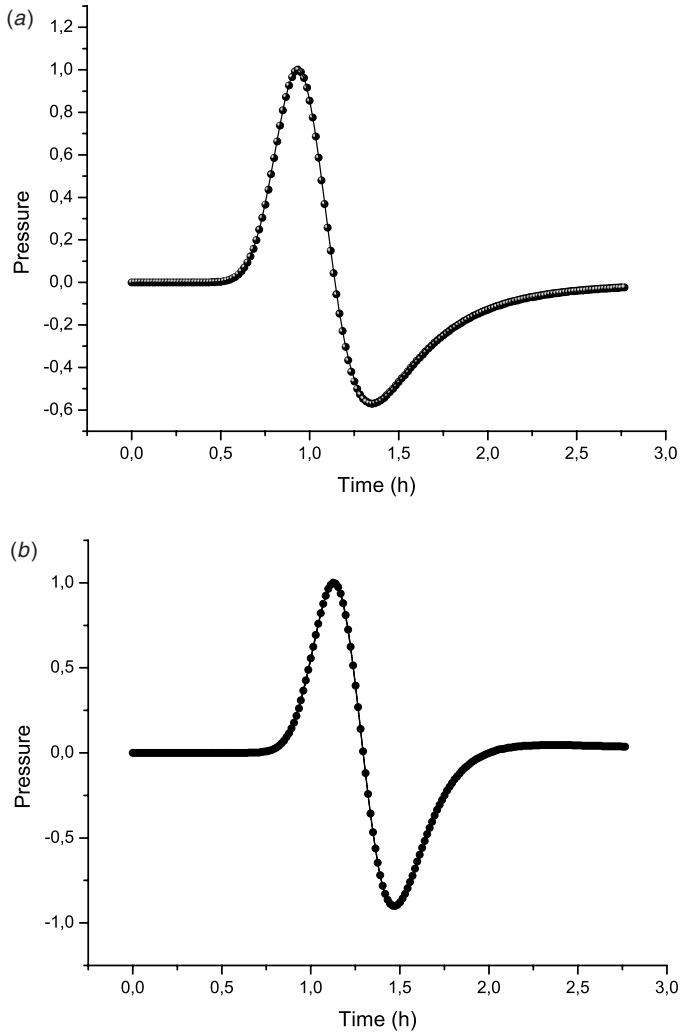

Figure 7. Comparison between the 2D analytical and numerical solutions (solid line and dots) for $\nu = 0.9$ (*a*) and $\nu = 1.5$ (*b*). A memory length $J = 10\,000$ time steps has been used in (*a*).

$f_p = 0.0005$ Hz $= f_0$. Figure 2 shows the comparison, ensuring that the frequency-domain approach to compute the Green function is correct and that we can use it to test the numerical modeling code for $\nu \neq 1$.

The pressure field for various values of ν is shown in figure 3, where we have considered the nD Green functions, the previous properties and parameters, $f_p = f_0$ and $\omega_0 = 2\pi f_0$, which corresponds to the reference frequency used in figure 1. We consider x, y and z such that the source–receiver radial distance is $r = 100$ m. In the 3D case, it is $\kappa_2 = \kappa_1$. The behavior of the pulse tends to be wave-like when $\nu \to 1.5$. If we assume that the location of the pulse is approximately given by the onset, we obtain 'traveltimes' of 0.3 h and 0.65 h for $\nu = 0.5$ and 1.5, respectively. This gives velocities of 330 m h^{-1} and 154 m h^{-1}, respectively, which are in qualitative agreement with the values of the energy velocities shown in figure 1(*b*), indicating that the energy velocity rather than the group velocity describes the

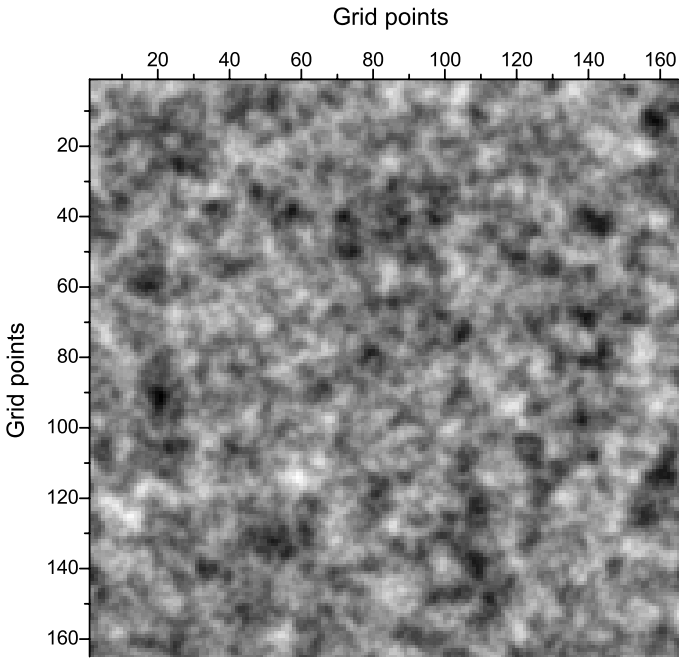

Figure 8. Fractal image of the porosity corresponding to a typical sandstone.

onset of the perturbation. Note that from equations (23) and (27), the energy velocity is proportional to $\omega^{1-\nu/2}$, i.e, $v_e \propto \omega^{3/4}$ for $\nu = 0.5$ and $v_e \propto \omega^{1/4}$ for $\nu = 1.5$. Hence, the velocity decreases with decreasing frequency. In the diffusion process, the pulse dominant frequency decreases, implying a slower propagation. This explains the differences observed between our calculations and the values given in figure 1(*b*).

The numerical simulations follow. In all the cases, the pressure field is normalized. We first consider the 1D case and 165 grid points, with $\Delta x = 10$ m. The time step given by equation (A.6), according to the stability condition, is shown in figure 4 as a function of ν, where $h < 0.3$ s for $\nu = 0.5$ and $h < 50$ s for $\nu = 1.5$. The GL derivative is obtained by considering the whole past history of the field. Then, the algorithm can be expensive for low values of ν. To test the accuracy of the time discretization, figure 5 compares the FD phase velocity and attenuation factor as a function of frequency to the exact values for two different memory lengths J, $\nu = 0.5$ and $h = 0.2$ s. The arrow indicates the peak source frequency used in the simulations. As can be seen, the approximation requires the whole history. Figure 6 compares the numerical and analytical solutions for $\nu = 0.5$ (*a*) and $\nu = 1.5$ (*b*), where $f_p = f_0$. The maximum time is 2.7 h with $h = 0.2$ s (50 000 steps) in (*a*), and $h = 5$ s (2000 steps) in (*b*). The dashed line corresponds to $J = 5000$, showing that the whole memory length has to be used. Next, we perform 2D simulations in the same medium, using a 165×165 mesh, with $\Delta x = \Delta z = 10$ m for $\nu = 0.9$ and 1.5. In the first case, $h = 1$ s and we compute 10 000 steps. Figure 7 compares the analytical and numerical solutions. Again, the agreement is excellent.

Finally, we compute a fluid-flow simulation in fractal media. We model fractal variations by using a von Kármán autocovariance probability function as described in appendix B. We consider a low-frequency source with a peak frequency $f_p = f_0$. The medium is described by $\phi_0 = 0.25$, $\Delta\phi_m = 0.05$, $l = 20$ m, $\epsilon = 0.18$ and $n = 2$. Figure 8 shows a map of the porosity.

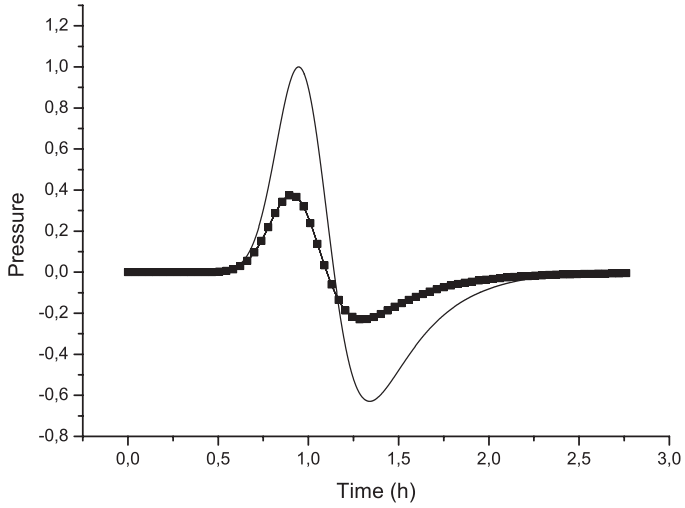

Figure 9. Pressure field in a fractal medium for $\nu = 0.9$ (solid line with symbols). For comparison the case with $\nu = 1$ is shown (solid line).

We assume $R = 10$ μm, $\kappa_1 = 4\kappa_3$, $\eta = 1$ cP, $K_s = 40$ GPa, $\mu_s = 3$ $K_s/5$ (Poisson solid), $A = 2$, $B = 3$ and $K_f = 2.25$ GPa. We consider $\nu = 0.9$ over the whole space and we use the same mesh of the previous simulation. The time step is $h = 1$ s and we compute 10 000 steps. The pressure at $x = z = 100$ m from the source location is shown in figure 9 (symbols), normalized with respect to the maximum value of the field for $\nu = 1$, displayed as a solid line.

As stated above, we consider the whole memory history. To solve this problem, which requires substantial memory storage, further research is necessary to verify if the fractional derivative can be computed with a suitable approximation [50, 57]. However, as shown in figure 5, the calculation requires all the past history and a local approximation of the time derivative would be inaccurate. The problem seems to be the correct approximation of the low-frequency components or later times of the signal (see figures 5(*b*) and 6(*a*), respectively) and this requires us to consider the whole past history of the field in the calculation of the GL summation. A solution could be to increase the time step with increasing time. The slowing down of the diffusion rate with time suggests that it is possible to increase the time step as time increases [25, 52], a method that has been re-discovered by Ford and Simpson [28] as the 'Nested meshed scheme'.

7. Conclusions

We have formulated a theory for anomalous fluid-pressure diffusion in inhomogeneous anisotropic media, based on a time-fractional diffusion equation. The flow is described by a time-dependent permeability of the form $t^{1-\nu}$, where t is the time and ν is the order of the fractional derivative. The coupling between the pressure and deformation of the frame is taken into account for the case of uniaxial strain conditions, through a modification of the stiffness. The physical quantities have been obtained by using a plane-wave kernel and concepts from wave propagation in anelastic media. In particular, we show that the envelope velocity (a kinematical quantity) is equal to the energy velocity (a dynamical quantity). This is not the case for waves. The group velocity is greater than the energy velocity, which represents the

location of the diffusion front. The relation between the energy angle and the phase angle depends on the ratio between the horizontal and vertical permeabilities, and therefore strong differences are expected between the flux and wavevector directions, compared to the seismic (propagation) case. We have also provided two definitions of a quality factor. These new implications are useful for tracking the diffusion front in reservoir rocks, where the signal travels at the energy velocity, as shown by the time response. Moreover, we have obtained the time-domain Green function in homogeneous 1D, 2D and 3D media.

The simulation of pressure diffusion in inhomogeneous media has been achieved by using the Grünwald–Letnikov derivative, storing the whole field to obtain accurate results. The algorithm has been tested with the 1D and 2D Green functions and applied to pressure diffusion in fractal porosity media, simulating realistic reservoir conditions.

The analysis of the physics and the simulation also applies to anomalous electromagnetic diffusion in view of the mathematical analogy between a fluid flow in porous media and electromagnetic low-frequency fields. Both phenomena are described by the time-fractional diffusion equation.

Acknowledgments

This paper has been partially funded by the CO_2 Monitor project. We thank Francesco Mainardi and two anonymous reviewers for useful comments.

Appendix A. FD stability and accuracy

Here, we analyze the numerical stability and accuracy of the numerical discretization.

A.1. Stability

The kernel $\exp(\mathrm{i}kx)$ replaced in equation (56) gives

$$p^n = -h^\nu b_1 k^2 p^{n-1} - \sum_{j=1}^{J} (-1)^j \binom{\nu}{j} p^{n-j}. \tag{A.1}$$

Let us assume the relation

$$p^j = g p^{j-1}, \tag{A.2}$$

where g is the amplification factor. Then

$$g = -h^\nu b_1 k^2 - \sum_{j=1}^{J} (-1)^j \binom{\nu}{j} g^{1-j}. \tag{A.3}$$

The von Neumann condition for stability implies

$$\max|g| \leqslant 1. \tag{A.4}$$

In particular, setting $g = -1$ and $k = \pi/\Delta x$, the Nyquist wavenumber, we obtain the following stability condition:

$$h \leqslant \left\{ \frac{\Delta x^2}{\pi^2 b_1} \left[1 + \sum_{j=1}^{J} \binom{\nu}{j} \right] \right\}^{1/\nu}. \tag{A.5}$$

It can be shown that the 3D condition is

$$h \leqslant \left\{ \frac{1}{\pi^2} \left(\frac{b_1}{\Delta x^2} + \frac{b_2}{\Delta y^2} + \frac{b_3}{\Delta z^2} \right)^{-1} \left[1 + \sum_{j=1}^{J} \binom{\nu}{j} \right] \right\}^{1/\nu}. \tag{A.6}$$

A.2. FD phase velocity and attenuation factor

Let us assume constant material properties, propagation along the x-direction and a field kernel $\exp(\mathrm{i}(\omega nh - kx)$, with $t = nh$ and k being the complex horizontal wavenumber component. The complex velocity is given by

$$\bar{v}_c = \frac{\omega}{k}. \tag{A.7}$$

Substituting this kernel into equation (56) gives

$$\bar{v}_c = \mathrm{i}\xi\sqrt{\frac{h^{\nu-2}b_1}{1+\Sigma}}\exp(-\mathrm{i}\xi/2) = \mathrm{i}\xi\sqrt{\frac{\xi_0^{\nu}N\kappa_1}{\eta h(1+\Sigma)}}\exp(-\mathrm{i}\xi/2), \tag{A.8}$$

where $\xi = \omega h$, $\xi_0 = \omega_0 h$ and

$$\Sigma = \sum_{j=1}^{J}(-1)^j\binom{\nu}{j}\exp(-\mathrm{i}j\xi). \tag{A.9}$$

Note that ξ and ξ_0 are dimensionless, N(Pa), κ_1(m^2), η(Pa . s) and h(s).

The FD phase velocity is given by

$$\bar{v}_p = \left[\mathrm{Re}\left(\frac{1}{\bar{v}_c}\right)\right]^{-1}, \tag{A.10}$$

while the attenuation factor is

$$\bar{\alpha} = -\omega\,\mathrm{Im}\left(\frac{1}{\bar{v}_c}\right) \tag{A.11}$$

to be compared with equations (23) to evaluate the accuracy of the time discretizations.

Appendix B. Modeling of fractal media

We vary the porosity fractally and compute the permeability components and elastic moduli from deterministic relations between these quantities and the porosity (see below).

Let $\Delta\phi_m$ be the maximum deviation of the porosity from the background value ϕ_0. The porosity at (x, y, z) is first subjected to the variations $(\Delta\phi)^r$, such that

$$-\Delta\phi_m \leqslant (\Delta\phi)^r \leqslant \Delta\phi_m, \tag{B.1}$$

where $(\Delta\phi)^r$ is obtained from a random number generator and the superindex 'r' denotes randomness. (Random numbers between 0 and 1 are generated and then scaled to the interval $[-1, 1]\Delta\phi_m$.)

Small-scale porosity variations in the reservoir can be described by the von Kármán autocovariance function [15, 59]. The corresponding wavenumber-domain power spectrum is

$$P(k_1, k_2, k_3) = K(1 + k^2a^2)^{-(\epsilon+n/2)}, \tag{B.2}$$

where $k = \sqrt{k_1^2 + k_2^2 + k_3^2}$ is the wavenumber, a is the correlation length, ϵ $(0 < \epsilon < 1)$ is a self-similarity coefficient, K is a normalization constant and n is the Euclidean dimension. The von Kármán correlation function describes self-affine, fractal processes of fractal dimension $n + 1 - \epsilon$ at scale smaller than a.

The porosity is then calculated as

$$\phi(x, y, z) = \phi_0 \pm \Delta\phi(x, y, z), \tag{B.3}$$

where

$$\widetilde{\Delta\phi}(k_1, k_2, k_3) = \widetilde{(\Delta\phi)}^r(k_1, k_2, k_3)P(k_1, k_2, k_3), \tag{B.4}$$

with $\widetilde{(\Delta\phi)}^r(k_1, k_2, k_3)$ being the Fourier transform of $(\Delta\phi)^r(x, y, z)$. (The tilde denotes the space Fourier transform.)

Porosity and vertical permeability are related by an equation derived by Carcione *et al* [14]

$$\kappa_3 = \frac{r_g^2\phi^3}{45(1-\phi)^2}, \tag{B.5}$$

where r_g denotes the average radius of the grains.

We use the Krief model, generalized to the anisotropic case [18], to obtain the dry-rock moduli,

$$\begin{aligned} c_{11} &= (K_s + 4\mu_s/3)(1-\phi)^{A/(1-\phi)}, \\ c_{12} &= (K_s - 2\mu_s/3)(1-\phi)^{A/(1-\phi)}, \\ c_{13} &= (K_s - 2\mu_s/3)(1-\phi)^{B/(1-\phi)}, \\ c_{33} &= (K_s + 4\mu_s/3)(1-\phi)^{B/(1-\phi)}, \end{aligned} \tag{B.6}$$

where A and B are constants. The use of two constants is somehow equivalent to vary the Krief exponent as a function of the propagation (phase) angle, since c_{11} and c_{12} describe the velocities along the stratification, and c_{13} and c_{33} along the perpendicular direction. It is $A < B$, indicating that the critical porosity value is larger for the elastic constants describing the properties along the layering, i.e., the skeleton is mainly defined by these constants at high porosity. Substituting equation (B.6) into equation (13) yields

$$K = \tfrac{1}{3}K_s[(1-\phi)^{A/(1-\phi)} + (1-\phi)^{B/(1-\phi)}], \tag{B.7}$$

while equation (12) gives

$$\alpha = 1 - (1-\phi)^{B/(1-\phi)}. \tag{B.8}$$

References

[1] Badea E A, Everett M E, Newman G A and Biro O 2001 Finite-element analysis of controlled-source electromagnetic induction using Coulomb-gauged potentials *Geophysics* **66** 786–99

[2] Barkai E, Metzler R and Klafter J 2000 From continuous-time random walks to the fractional Fokker–Planck equation *Phys. Rev.* E **61** 132–8

[3] Bear J 1988 *Dynamics of Fluid Flow in Porous Media* (New York: Dover)

[4] Berkowitz B J, Klafter J, Metzler R and Scher H 2002 Physical pictures of transport in heterogeneous media: advection-dispersion, random-walk and fractional derivative formulations *Water Resources Res.* **38** 1191

[5] Biot M A 1962 Mechanics of deformation and acoustic propagation in porous media *J. Appl. Phys.* **33** 1482–98

[6] Caputo M and Carcione J M 2011 Hysteresis cycles and fatigue criteria using anelastic models based on fractional derivatives *Rheol. Acta* **50** 107–15

[7] Caputo M, Carcione J M and Cavallini F 2011 Wave simulation in biological media based on the Kelvin–Voigt fractional-derivative stress–strain relation *Ultrasound Med. Biol.* **37** 996–1004

[8] Caputo M and Mainardi F 1971 Linear models of dissipation in anelastic solids *Riv. Nuovo Cimento* II **1** 161–98

[9] Caputo M and Plastino W 2004 Diffusion in porous layers with memory *Geophys. J. Int.* **158** 385–96

[10] Carcione J M 1994 Wavefronts in dissipative anisotropic media *Geophysics* **59** 644–57

[11] Carcione J M 2006 A spectral numerical method for electromagnetic diffusion *Geophysics* **71** I1–9

[12] Carcione J M 2007 *Wave Fields in Real Media. Theory and Numerical Simulation of Wave Propagation in Anisotropic, Anelastic, Porous and Electromagnetic Media* (Amsterdam: Elsevier)

[13] Carcione J M 2009 Theory and modeling of constant-Q P- and S-waves using fractional time derivatives *Geophysics* **74** T1–T11

[14] Carcione J M, Cavallini F, Mainardi F and Hanyga A 2002 Time-domain modeling of constant-Q seismic waves using fractional derivatives *Pure Appl. Geophys.* **159** 1719–36

[15] Carcione J M, Finetti I and Gei D 2003 Seismic modeling study of the Earth's deep crust *Geophysics* **68** 656–64

[16] Carcione J M and Gei D 2009 Theory and numerical simulation of fluid-pressure diffusion in anisotropic porous media *Geophysics* **74** N31–N39
[17] Carcione J M, Gurevich B and Cavallini F 2000 A generalized Biot–Gassmann model for the acoustic properties of Shaley sandstones *Geophys. Prospect.* **48** 539–57
[18] Carcione J M, Helle H B and Avseth P 2011 Source-rock seismic-velocity models: Gassmann versus Backus *Geophysics* **76** N37–N45
[19] Carslaw H S and Jaeger J C 1959 *Conduction of Heat in Solids* (Oxford: Clarendon)
[20] Chandler R N and Johnson D L 1981 The equivalence of quasi-static flow in fluid-saturated porous media and Biot's slow wave in the limit of zero frequency *J. Appl. Phys.* **52** 3391–5
[21] Compte A 1996 Stochastic foundations of fractional dynamics *Phys. Rev.* E **53** 4191–3
[22] Detournay E and Cheng A H D 1993 Comprehensive rock engineering: principles, practice and projects *Fundamentals of Poroelasticity* vol 2 ed C Fairhurst (New York: Pergamon) pp 113–71
[23] Diethelm K 2010 *The Analysis of Fractional Differential Equations* (Berlin: Springer)
[24] Diethelm K, Ford N J, Freed A D and Luchko Yu 2005 *Comput. Methods Appl. Mech. Eng.* **194** 743–73
[25] Douglas J Jr and Gallie T M Jr 1955 Variable time steps in the solution of the heat flow equation by a difference equation *Proc. Am. Math. Soc.* **6** 787–93
[26] Eidesmo T, Ellingsrud S, MacGregor L M, Constable S, Sinha M C, Johansen S, Kong F N and Westerdahl H 2002 Sea bed logging (SBL), a new method for remote and direct identification of hydrocarbon filled layers in deepwaters areas *First Break* **20** 144–51
[27] Fedotov S 2010 Non-Markovian random walks and nonlinear reactions: subdiffusion and propagating fronts *Phys. Rev.* E **81** 011117
[28] Ford N J and Simpson C 2001 The numerical solution of fractional differential equations: speed versus accuracy *Numer. Algorithms* **26** 333–46
[29] Gorenflo R 1997 Fractional calculus, some numerical methods *Fractals and Fractional Calculus in Continuum Mechanics* ed A Carpinteri and F Mainardi (Wien: Springer) pp 277–90
[30] Gorenflo R, Mainardi F, Moretti D, Pagnini G and Paradisi P 2002 Discrete random walk models for space-time fractional diffusion *Chem. Phys.* **284** 521–41
[31] Grünwald A K 1867 Über 'begrenzte' Derivationen und deren Anwendung *Z. Angew. Math. Phys.* **12** 441–80
[32] Gutierrez M S and Lewis R W 2002 Coupling of fluid flow and deformation in underground formations *J. Eng. Mech.* **128** 779–87
[33] Hanyga A 2002 Multidimensional solutions of time-fractional diffusion-wave equations *Proc. R. Soc. Lond.* A **458** 933–57
[34] Helbig K 1994 *Foundations of Anisotropy for Exploration Seismics* (Oxford: Pergamon)
[35] Henry B I, Langlands T A M and Straka P 2010 Fractional Fokker–Planck equations for subdiffusion with space-and-time dependent forces *Phys. Rev. Lett.* **105** 070602
[36] Henry B I, Langlands T A M and Wearne S L 2006 Anomalous diffusion with linear reaction dynamics: from continuous time random walks to fractional reaction-diffusion equations *Phys. Rev.* E **74** 031116
[37] Hilfer R and Anton L 1995 Fractional master equations and fractal time random walks *Phys Rev.* E **51** 848–51
[38] Iaffaladano G, Caputo M and Martino S 2006 Experimental and theoretical memory diffusion of water in sand *Hydrol. Earth Syst. Sci.* **10** 93–100
[39] Jiang X and Qi H 2012 Thermal wave model of bioheat transfer with modified Riemann–Liouville fractional derivative *J. Phys. A: Math. Theor.* **45** 485101
[40] Kosloff D and Baysal E 1982 Forward modeling by the Fourier method *Geophysics* **47** 1402–12
[41] Krief M, Garat J, Stellingwerff J and Ventre J 1990 A petrophysical interpretation using the velocities of P and S waves (full waveform sonic) *Log Anal.* **31** 355–69
[42] Letnikov A V 1868 Theory of differentiation of fractional order *Mat. Sb.* **3** 1–68 (in Russian)
[43] Lin Y and Xu C 2007 Finite difference/spectral approximations for the time-fractional diffusion equation *J. Comput. Phys.* **225** 1533–52
[44] Luzón F, García-Jerez A, Santoyo M A and Sánchez-Sesma F J 2010 Numerical modelling of pore pressure variations due to time varying loads using a hybrid technique: the case of the Itoiz reservoir (northern Spain) *Geophys. J. Int.* **180** 327–38
[45] Metzler R and Klafter J 2000 The random walk's guide to anomalous diffusion: a fractional dynamics approach *Phys. Rep.* **339** 1–77
[46] Mainardi F 1995 The time-fractional diffusion equation *Radiophys. Quantum Electron.* **38** 13–24
[47] Mainardi F 1996 Fractional relaxation-oscillation and fractional diffusion-wave phenomena *Chaos Solitons Fractals* **7** 1461–77
[48] Mainardi F, Luchko Y and Pagnini G 2001 The fundamental solution of the space-time fractional diffusion equation *Fractional Calculus Appl. Anal.* **4** 153–92
[49] Mainardi F and Paradisi P 2001 Fractional diffusive waves *J. Comput. Acoust.* **9** 1417–36

[50] Murio D A 2008 Implicit finite difference approximation for time fractional diffusion equations *Comput. Math. Appl.* **56** 1138–45
[51] Nigmatullin R R 1986 Realization of the generalized transfer equation in a medium with fractal geometry *Phys. Status Solidi* b **133** 425–30
[52] Oristaglio M L and Hohmann G W 1984 Diffusion of electromagnetic fields into a two-dimensional earth: a finite-difference approach *Geophysics* **49** 870–94
[53] Pilant W L 1979 *Elastic Waves in the Earth* (Amsterdam: Elsevier)
[54] Schumer R, Meerschaert M M and Baeumer B 2009 Fractional advection-dispersion equations for modeling transport at the Earth surface *J. Geophys. Res.* **114** F00A07
[55] Shapiro S A, Rothert E, Rath V and Rindschwentner J 2002 Characterization of fluid transport properties of reservoirs using induced microseismicity *Geophysics* **67** 212–20
[56] Sokolov I M and Klafter J 2006 Field-induced dispersion in subdiffusion *Phys. Rev. Lett.* **97** 140602
[57] Torres F, Vaudon P and Jecko B 1996 Application of fractional derivatives to the FDTD modeling of pulse propagation in a Cole–Cole dispersive *Microw. Opt. Technol. Lett.* **13** 300–4
[58] Trinks C and Ruge P 2002 Treatment of dynamic systems with fractional derivatives without evaluating memory-integrals *Comput. Mech.* **29** 471–6
[59] von Kármán T 1948 Progress in the statistical theory of turbulence *J. Mar. Res.* **7** 252–64
[60] Westerlund S 1991 Dead matter has memory! *Phys. Scr.* **43** 174–9